Materials Research Bulletin, Volume 44, Issue 6, 3 June 2009, Pages 1219-1224

Accepted Manuscript

Title: Impact of Zr/Ti ratio in the PZT on the photoreduction of silver nanoparticles

Authors: D. Tiwari, S. Dunn

PII: S0025-5408(09)00031-2
DOI: doi:10.1016/j.materresbull.2009.01.016
Reference: MRB 4383

To appear in: *MRB*

Received date: 11-11-2008
Revised date: 6-1-2009
Accepted date: 22-1-2009

Please cite this article as: D. Tiwari, S. Dunn, Impact of Zr/Ti ratio in the PZT on the photoreduction of silver nanoparticles, *Materials Research Bulletin* (2008), doi:10.1016/j.materresbull.2009.01.016

Impact of Zr/Ti ratio in the PZT on the photoreduction of silver nanoparticles

D Tiwari[a)] and S Dunn, Building 30, Nanotechnology Centre, Cranfield University, Cranfield, MK43 0AL, UK.

Corresponding author email – d.tiwari@cranfield.ac.uk

Abstract: Silver nanoparticle deposition from an aqueous solution of silver nitrate onto the surface of PZT thin films of stoichiometric compositions $PbZr_{0.3}Ti_{0.7}O_3$ and $PbZr_{0.52}Ti_{0.48}O_3$ has been investigated. The impact of Zr/Ti ratio on the photochemical properties of PZT is shown by the preferential growth of silver nanoparticles onto the surface. Photoreduction of silver occurs on both c^+ and c^- domains on a $PbZr_{0.52}Ti_{0.48}O_3$ whereas it occurs only on c^+ domains on a $PbZr_{0.3}Ti_{0.7}O_3$ surface. The difference in deposition pattern is attributed to difference in magnitude of spontaneous polarization, effective hole concentration and band gap of the two samples which impacts shape and width of space charge layer in the two samples resulting in a change in band bending at the surface.

Keywords: A. semiconductors; A. nanostructures; D. surface properties; D. ferroelectricity

1. Introduction: Nanostructured materials and systems have generated intense scientific and technological interest over the last few years because of their unique properties and potential applications in areas as diverse as electronics, optics, information storage, bio-medicine, sensors and product labelling. A variety of interesting approaches have been developed for the growth of nanostructures one of them is ferroelectric nanolithography [1],

which facilitates the growth of 3D nanostructures on predefined locations on a ferroelectric surface.

Ferroelectric materials are now considered and treated as wide band gap semiconductors rather than insulators [2]. In ferroelectric materials such as lead zirconate titanate ($PbZr_xTi_{1-x})O_3$ a polarization bound charge exists in the vicinity of surfaces and interfaces which is compensated by internal and/or external screening. External screening involves surface adsorption of oppositely charged molecules or ions from the atmosphere on the surface of the ferroelectric. Molecules with a dipole can also orient themselves on the surface to screen charge. Internal screening involves compensation of surface polarisation charge by defects and free charge carriers in the bulk of the material and takes the form of space charge region (SCR) due to 'band bending' at the surface [3].

When a photosensitive material such as a ferroelectric is exposed to high energy UV light, photoexcited charge carriers (e^--h^+) pairs are generated in both the surface layer and the bulk of the film as deep as the absorption limit. These charge carriers are driven apart by the internal electric field in the SCR. In the positively polarised domains electrons are forced to migrate towards the surface [4] and in negatively polarised domains electrons move away from the surface and towards the bulk. When the ferroelectric surface is dipped in a silver salt ($AgNO_3$) solution and exposed to UV light, the metal cations can react with photoexcited electrons available on c^+ domains and are reduced to silver metal. It is also possible to produce PbO by oxidation of lead salts on the negatively poled domains. The photoreduction and photoxidation

reactions on c^+ and c^- domains are described by reactions 1 and 2 respectively.

$$Ag^+ + e^- \longrightarrow Ag^0 \quad (1)$$

$$Pb^{2+} + 2H_2O + 2h^+ \longrightarrow PbO_2 + 4H^+ \quad (2)$$

On a positive (c+) domain the Ag^+ ions should not be intimately attached to the c^+ surface and in fact the negatively charged counter ions would be forming a Stern or double layer [5]. Therefore there was a tunnelling mechanism that was allowing the electrons to pass through the bound ions and reduce the metal cations to metal. Recent works by Giocondi and Rohrer [6] shows that similar domain specific reactivity exists on the surfaces of ferroelectric microcrystal owing to the existence of dipolar field effect. Similar spatially selective oxidation and reduction reactions were observed on non ferroelectric $SrTiO_3$ surfaces [7].

The growth of metallic nanostructures on ferroelectric materials has been shown to be dependent on a number of surface phenomena such as grain boundaries [8], ferroelectric domains [1] and domain boundaries [9]. The photochemical reactivity of ferroelectric surfaces is not only dependent on polarization of domain that is underlying the surface [10] but also the crystallographic orientation of the sample [11] and the density of defects in the sample [9] [12].

Many studies on the structural, electrical [13] [14]and optical properties [15] of PZT films of different stoichiometric compositions have been reported but very limited information exists on the photochemical properties of different composition of PZT. The compositions used here are $PbZr_{0.3}Ti_{0.7}O_3$ and $PbZr_{0.52}Ti_{0.48}O_3$; the crystallographic structure at room temperature according

to bulk phase diagram is tetragonal (space group P4mm) and coexistence of tetragonal and rhombohedral (morphotropic phase boundary) respectively. Investigations show that PZT 52/48 possess a higher piezoelectric coefficient than PZT 30/70 because of the increased ease of reorientation during poling. Coupling factor and dielectric constant are also found to be highest near the morphotropic phase boundary. We have investigated the photochemical properties of PZT thin films of different stoichiometric compositions by carrying out the Ag nanocluster deposition experiments using two UV lamps of different intensities. We have focussed on the nature and reasons behind the preferential growth of nanoparticles on patterned PZT. Therefore by tracking the change in the Ag nanoparticle deposition we are generating a handle for understanding the impact of Zr/Ti ratio in the PZT on the photochemical reactivity at the surface. The difference in deposition pattern is attributed to the difference in the magnitude of spontaneous polarization, effective hole concentration and the band gap of the two samples which impacts the shape and width of space charge region (SCR) in the two samples resulting in a change in the band bending at the surface.

2. Experimental

PZT films, with the Zr/Ti ratio of 30/70 and 52/48 were made using a sol-gel process. The sols were prepared according to previously published work [16]. The substrate was prepared by sputtering Pt (100 nm)/Ti (5 nm) onto Si wafer. The sol was then spin coated onto the substrate. The sample was processed according to previously published work [16] [17] and gave a PZT film that was 70 nm thick. In each case the sample was 2 cm^2 in area. Film

orientation was determined using X-ray diffraction measurement on a Siemens D5005 diffractometer using CuKα radiation.

The samples were poled using a modified DI 3000 Atomic Force Microscope (AFM) system in PFM [18] mode using a conductive cantilever (a Veeco contact mode cantilever made of Antimony doped Si, resonant frequency 130-250 kHz). The base electrode of the sample was obtained by scratching a part of the sample and connecting using silverdag. For poling the cantilever and the sample base electrode were connected to a DC power supply set at 12V. The pattern produced was a series of squares of reduced dimensions set inside each other of opposite domain orientation

A fresh solution of 0.01M $AgNO_3$ was prepared. A drop of this solution, which was filtered using a 0.2 μm filter, was put over the poled pattern. The sample was irradiated with a UV lamp for 20 minutes. Two UV lamps a Honle 400 W Hg lamp (H lamp) and a Honle 400 W Fe-doped Hg lamp (F lamp) both giving irradiation from 200-400 nm (6.2-3.1 eV) have been used in our experiments [19]. The spectrum of 'H' and 'F' lamps are shown in figure 1. The emission spectrum for 'H' lamp indicates that it is a higher energy lamp compared to 'F' lamp because of its higher flux of photons above the band gap energy. After irradiation the samples were rinsed in deionised water and blow dry with N_2. The samples were imaged using a Philips XL30 SFEG scanning electron microscope. In each case the presence and absence of silver was confirmed using the EDX technique. The EDX software was first calibrated using a standard Co sample and then the percentage deposition of Ag was calculated in small areas on all the samples. The experiments were repeated on five

different PZT samples of each composition and same results were obtained on all samples of a composition.

3. Results and Discussion

XRD patterns of PZT (30/70) and PZT (52/48) are shown in figure 2. The preferred orientation in both the films is calculated using the intensities of the (111), (100) and (110) peak and the following equation:

$$I_{(xyz)} = \frac{I_{(xyz)}}{I_{(111)} + I_{(100)} + I_{(110)}} \quad (3)$$

Upon comparison of relative intensities it was found that PZT (30/70) is highly (111) oriented whereas in PZT (52/48) about 30% of crystals are (100) orientated and 70% are (111) orientated. The growth of PZT films is nucleation controlled and the orientation of PZT films is based on the substrate used. The reason for the less well (111) orientation of PZT 52/48 is due to the increase in lattice mismatch between the (111) - oriented Pt and (111)-oriented PZT with the increase in Zr content. The XRD pattern also shows absence of any intermediate pyrochlore phase in both samples. Figure 3 show that both the PZT samples have discrete grains with a random orientation across the surface before poling. The grain size in PZT 52/48 is larger than the grain size in PZT 30/70 this is because the grain sizes of PZT films strongly depend on the composition ratio via different nucleation/growth energy. The films with higher Ti content have smaller nucleation energy and therefore smaller size of the grains [20]. A typical PFM image of the poled pattern is shown in figure 4.

The patterned PZT surface immersed in silver nitrate solution was placed inside a UV box fitted with the 'F' or the 'H' lamp (as defined earlier) and irradiated for 20 min. The SEM images of photodeposited silver are shown in figure 5. Upon irradiation with 'F' lamp PZT 52/48 showed deposition of silver only on c^+ domains and no deposition on c^- domains. Whereas when high energy photons from 'H' lamp were used to irradiate the surface silver nanoparticles were deposited on both c^+ domains and the c^- domains. The size of silver particles on c^- domains is smaller and deposition is less dense compared to the c^+ domain. On a PZT 30/70 sample upon irradiation with 'F' lamp a similar deposition pattern is observed with silver present in c^+ and absent on c^- domains and when the 'H' lamp was used the deposition on c^+ domains increased significantly whereas no silver deposited on c^- domains. In our previous work we have reported photoreduction of various metals on c^+ domain following the band gap theory and strong band bending near the surface [5] [19]. However, Kitamura *et al* [24] have concluded that photovoltaic effect causes Ag deposition on +Z surface of $LiNbO_3$. Factors such as location of conduction band with respect to vacuum and size of band gap have a major impact on photochemical properties of a material [5]. Preferential deposition of metal on the surface of ferroelectric is found to be dependent not only on the polarization of domain underlying the surface [10] but also on the surface defects such as grain boundaries, domain boundaries and defects within the film [7]. Nanoparticles grow from discrete nucleation points across the surface. Existence of strong electric field at grain boundaries and domain boundaries influences the availability of photoexcited electrons and holes for photochemical reaction. The energy of UV irradiation also

influences the band structure and space charge layer at the surface. Upon illumination with high energy, restructuring of bands at the surface and narrowing of space charge region has also been reported [19]. In addition to above factors crystallographic orientation of the sample, magnitude of spontaneous polarization, effective hole concentration, size of grains in the two samples also influence photochemistry at the surface.

According to investigations by Pintilie *et al* [21] on a set of metal-Pb(Zr_xTi_{1-x})O_3 –metal samples with different Zr/Ti ratios (from 92/8 to 20/80), the variation in the width of interface layer δ is dependent on saturation polarization P_s, hole concentration p(T) and effective space-charge density in the depleted layer (N_{eff})of the sample. P_s for PZT 55/45 and 30/70 is reported to be 31.1 μC/cm^2 and 16 μC/cm^2 respectively and the hole concentration reported to be 2.2×10^{17} and 22×10^{17} cm^{-3} in that order. The thickness of the SCR is calculated to be 12.1 and 22.6 nm of 55/45 and 30/70 respectively. PZT 55/45 and 52/48 both have nearly same stiochiometric composition therefore we can say that the width of SCL in PZT 52/48 is roughly half of the same in PZT 30/70. According to the above data the band structure at the surface can be represented as shown in figure 6. The position of Fermi level is drawn towards the valence band in the above diagram because according to defect chemistry a non doped PZT film is a p type of semiconductor[13] since the naturally occurring impurities are acceptor impurities such as Al^{3+}, Na^+ and Fe^{3+}.

The band gap of PZT is between 3.2-3.7 eV [2]. The optical band gap energy of the PZT thin films is a composition dependent parameter and has been found to decrease with increase in Ti content [22]. The shift in band gap with

change in composition of PZT is due to the difference in radii of Zr^{2+} ions(r=.086nm) and Ti^{2+}ions(r=.09 nm). Therefore when Zr^{2+} is substituted for Ti^{2+}, Zr^{2+} ions occupy the lattice sites of the Ti^{2+} ions creating a decrease in the lattice parameters and films with higher packed density. Therefore the band gap energy of PZT 52/48 is found to be higher than 30/70 [22]. When the surface of PZT (52/48) is irradiated with low energy 'F' lamp photoreduction reaction occurs on the c^{+} domains due to the availability of photoexcited electrons at the surface. The grains in our 52/48 sample are big in size and therefore there are less nucleation points available for the growth of nanoparticles. This means that the deposited silver should be less dense and with bigger particle size compared to PZT 30/70 sample which has smaller grains. SFEG analysis shows that the silver deposition on the c^{+} domain of 52/48 sample was less dense with smaller particle size compared to the same on 30/70 sample. This can be attributed to the higher band gap energy of 52/48 sample and therefore reduced flux of photons that are above band gap are striking the surface resulting in fewer photoexcited electrons for photoreduction. No silver deposition was seen on the c^{-} domains because of the electric field in the SCR moved the photoelectrons away from the surface and the width of the SCR was large enough to prevent the electrons from penetrating it and reaching the surface.

When 'H' lamp is used to irradiate the surface an increased number of photoexcited electron-hole pairs are generated; an increased number of electron availability in the conduction band for photoreduction leads to a significant increase in silver nanoparticle deposition on the surface of both PZT 52/48 and PZT 30/70. The photogenerated electron-hole pairs also

contribute to internal screening at the surface and reduce the width of SCR eventually leading to a change in band structure at the surface [19] as shown in figure 7.

This reduction in the width of SCR has a major impact on the photochemical reactivity of a surface. Tunnelling is expected to occur at the semiconductor-electrolyte interface when the barrier, represented by the space charge region is sufficiently narrow [25]. Tunnelling between levels far from the barrier top occurs with a low probability but without considerable thermal activation whereas passage through the conduction band involves small barriers but requires thermal activation [26]. Tunnelling is thus more important, the higher and narrower the barrier. On a c^- domain the shape of the space charge layer prevents efficient mobility of the electron into the solution and there is a real energy barrier to the movement of the electron. But with the reduction in the width of SCR electrons can tunnel across the SCR to react with cations in solution. The penetrability of the electrons across the potential barrier increases by the relation given in equation 3. In PZT 52/48 the width of SCR is relatively less (50% to that on a 30/70 sample) and is further reduced upon exposure to high energy UV lamp therefore in order to penetrate across the SCR the photoexcited electrons have to travel a much less distance (half the distance as compared to 30/70) and therefore the probability of photoexcited electrons tunneling across the negatively charged surface and getting photo reduced to produce Ag^0 is heavily increased.

The penetrability T of a barrier of height E and width w can be calculated approximately by [23]:

$$T = e^{-2\alpha w} \qquad (4)$$

$$\alpha = \frac{1}{\hbar}\sqrt{2mE} \quad (5)$$

Where $\hbar$ is the Quantum of angular momentum = 1.05×10^{-34},

m is the electron mass= 9.1×10^{-31},

w is the width of SCR and is12.1 and 22.6 nm for 52/48 and 30/70 respectively, potential barrier E for PZT (52/48) and PZT(30/70) is 1.09eV and 1.37eV resp. Therefore using eq. (5)

$\alpha_{52/48}$ = 5.365×10^{9} $m^{-1}$and

$\alpha_{30/70}$ = 6.015×10^{9} m^{-1}

Using eq. (4) the penetrability

$T_{52/48}$ = 4.17×10^{-57} and

$T_{30/70}$ = 8.65×10^{-119}

Which means that the probability of electrons penetrating across the PZT(52/48) SCR is about 10^{62} times greater than across the PZT(30/70) SCR. Also upon irradiation with higher energy photons, for every 1 nm decrease in the SCR of both the samples the penetrability increases by a factor of 10^5 and 10^6 in PZT 52/48 and 30/70 respectively. In a PZT 52/48 sample very high penetrability across the SCR due to reduction in width of SCR results deposition of silver on both c+ and c- domains. However due to the negative polarisation charge present on the surface of the c- domain and the electric field associated with this polarisation charge the actual number of electrons tunnelling across the potential barrier is greatly reduced. This explains the reason why the silver nanocluster deposition on c- domain is less than the c+ domain in PZT 52/48.

Our previous work emphasizes on the impact of crystallographic orientation of the PZT on the photo deposition of Ag nanoparticles [11]. It was found that

upon exposed to UV light silver deposited in [100] faces and not in [111]. XRD of PZT 52/48 confirms that about 30% of crystals are [100] orientated and 70% are [111] orientated. Therefore it is possible that the deposition of silver is occurring in [100] faces in c- domains and [100] and [111] faces in c+ domains on our PZT 52/48 sample. Absence of any [100] orientation in PZT 30/70 explains why we do not see any silver deposition on c- domains of PZT 30/70.

4. Conclusion

We have investigated the photochemistry of PZT films of different stoichiometric compositions and shown that a variation in the Zr/Ti ratio has an influence on the photochemical reactivity of the material. The influence of semi-conducting properties of PZT on the photo-chemical/physical properties is also shown. The variation in the magnitude of spontaneous polarization, effective hole concentration and the band gap of the two samples was found responsible for the restructuring of valence and conduction bands at the surface eventually leading to changes in silver metal deposition.

References

[] S. V. Kalinin, D. A. Bonnell, T. Alvarez, X. Lei, Z. Hu, J. H. Ferris, Q. Zhang and S. Dunn, *Nano Letters* **2** (2002), pp. 589-593.

[2] I. Boerasu, L. Pintilie, M. Pereira, M. I. Vasilevskiy and M. J. M. Gomes, *J. Appl. Phys.* **93** (2003), pp. 4776-83.

[3] V M Fridkin, *Ferroelectric Semiconductors.* New York: Consultants Bureau, 1980.

[4] S. V. Kalinin and D. A. Bonnell, *Nanoscale Phenomenon in Ferroelectric Thin Films.* Dordrecht: Kluwer Academic Publishers, 2004.

[5] P. Jones, D. E. Gallardo and S. Dunn, Chem. Mater. **20** (2008), pp. 5901-5906.

[6] J. L. Giocondi and G. S. Rohrer, Topics in catalysis **49** (2008), pp. 18-23.

[7] J. L. Giocondi and G. S. Rohrer, J. Amer. Ceram. Soc. **86** (2003), pp.1182-1189.

[8] P. Jones and S. Dunn, *Nanotechnology* **18** (2007), pp. 185702.

[9] J. N. Hanson, B. J. Rodriguez, R. J. Nemanich and A. Gruverman, *Nanotechnology* **17** (2006), pp. 4946-4949.

[10] J. L. Giocondi and G. S. Rohrer, *Chem. Mater.* **13** (2001), pp. 241-242.

[11] S. Dunn, D. Tiwari, P. M.Jones and D. E. Gallardo, *J. Mater. Chem.* **17** (2007), pp. 4460-4463.

[12] S. Dunn and D. Tiwari, *Appl. Phys. Lett*. **93**, (2008), pp 092905.

[13] J F Scott, *Ferroelectric Memories.* New York: Springer, 2000.

[14] Xu Y, *Ferroelectric Materials and their Applications.* Amsterdam: Elsevier Science Pub Co, 1991.

[15] S. Trolier-McKinstry, J. Chen, K. Vedam and R. E. Newnham, *J. Am. Ceram. Soc.* **78** (1995), pp. 1907-1913.

[16] Q. Zhang and R. W. Whatmore*, J. Phys. D: Appl. Phys*. **34** (2001), pp. 2296-2301.

[17] J. M. Marshall, S. Corkovic, Q. Zhang, R. W. Whatmore, C. Chima-Oreke, W. L. Roberts, A. J. Bushby and M. J. Reece, *Integrated Ferroelectr.* **80** (2006), pp. 77-85.

[18] S. Dunn and R. W. Whatmore, *Integrated Ferroelectr.* **38** (2001), pp. 39-47.

[19] S. Dunn, P. M. Jones and D. E. Gallardo, *J. Am. Chem. Soc.* **129** (2007), pp. 8724-8728.

[20] K. Matsuura, K. Takai, T. Tamura, H. Ashida and S. Otani, *IEICE Trans. Electron.* **E81-C** (1998), pp. 528-536.

[21] L. Pintilie, I. Boerasu, M. J. M. Gomes, T. Zhao, R. Ramesh and M. Alexe, *J. Appl. Phys.* **98** (2005), pp. 124104-124112.

[22] S. Yang, D. Mo and X. Tang, *J. Mater. Sci.* **37** (2002), pp. 3841-3845.

[23] A. P. French and E. F. Taylor, *An Introduction to Quantum Physics* Anonymous London: Chapman & Hall, 1995.

[24] L. Xiaoyan, K. Kitamura, K. Terabe, H. Hatano, and N. Ohashi, *Appl. Phys. Lett*. **91**, (2007), pp 044101.

[25] J. Ulstrup, Surface Science **101** (1980), pp. 564-582.

[26] R.R. Dogonadze, A.M. Kuznetsov and J. Ulstrup, Electrochim. Acta **22** (1977), pp. 967.

Figure 1 Spectrum of ‘H’ and ‘F’ lamps used in experiments

Figure 2 XRD patterns of PZT (30/70) and PZT (52/48)

Figure 3 AFM image showing grain structure of PZT30/70 (left) and PZT52/48(right). The area of scanned region is 1.5 μm×1.5 μm.

Figure 4 A typical PFM image of the poled pattern. Brighter squares in the picture are positive domains and the dark squares are negative domains, surrounding region is an unpoled area.

Figure 5(a) PZT (52/48) upon irradiation with ‘F’ lamp(b) PZT (30/70) upon irradiation with ‘F’ lamp (c) PZT (52/48) upon irradiation with ‘H’ lamp (d) PZT (30/70) upon irradiation with ‘H’ lamp

Figure 6 Band structure of PZT 52/48 (solid lines), and PZT 30/70 (dashed lines) on a c^+ and c^- domain where Ec is the conduction band, Ev is the valence band, E_f is the fermi level. Ps arrow represents the direction of spontaneous polarisation. The W52/48 and W30/70 arrows represent the width of the SCR in both the samples.

Figure 7 Change in band structure upon irradiation with high energy ‘H’ lamp. The arrows represent the reduced width of SCR on the surface of PZT.

Figure 1

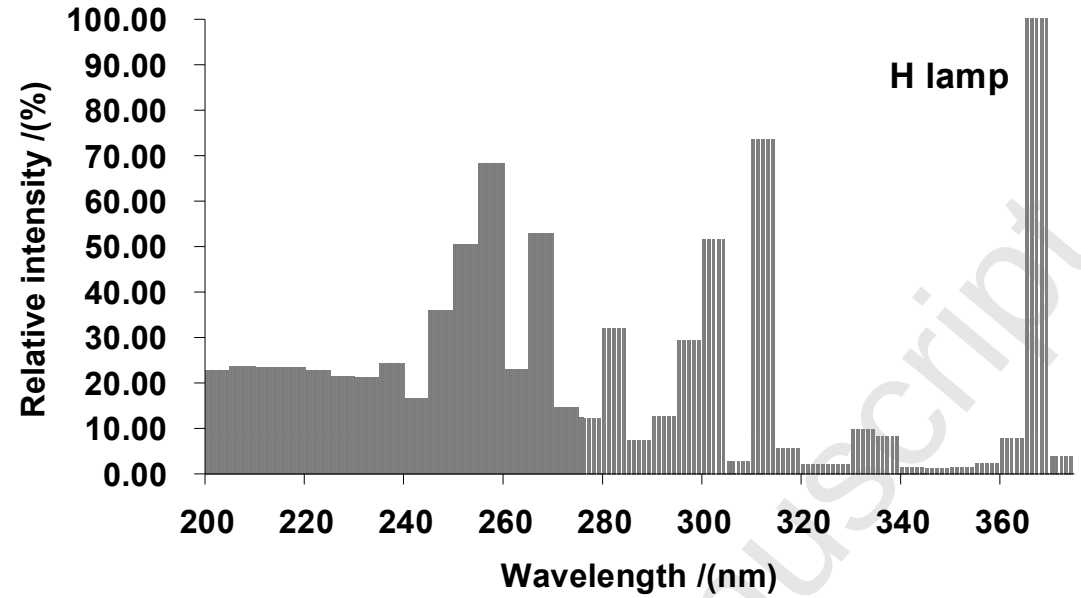

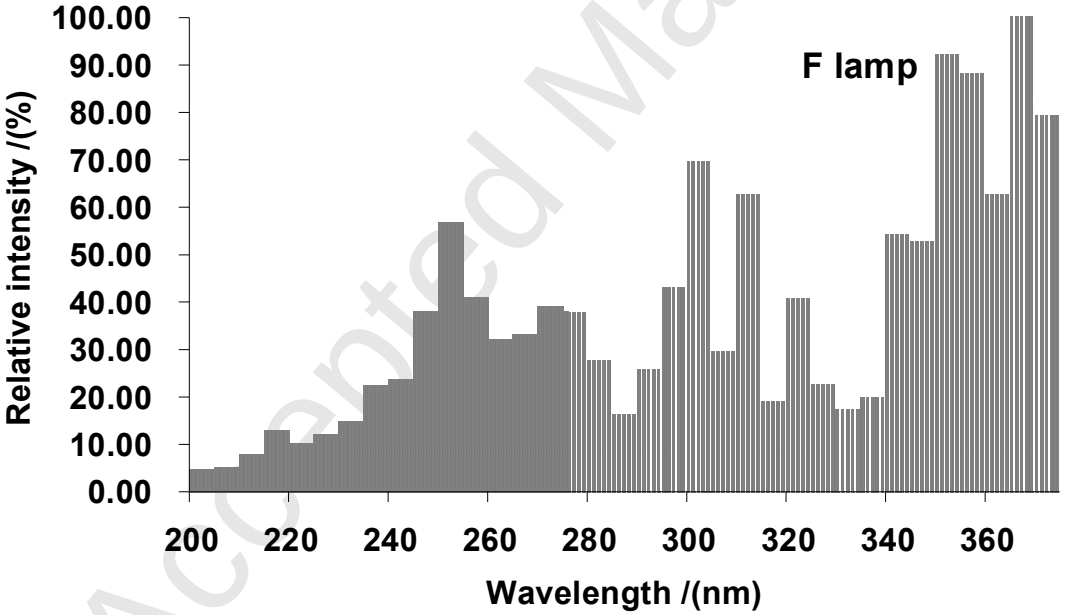

Figure 2

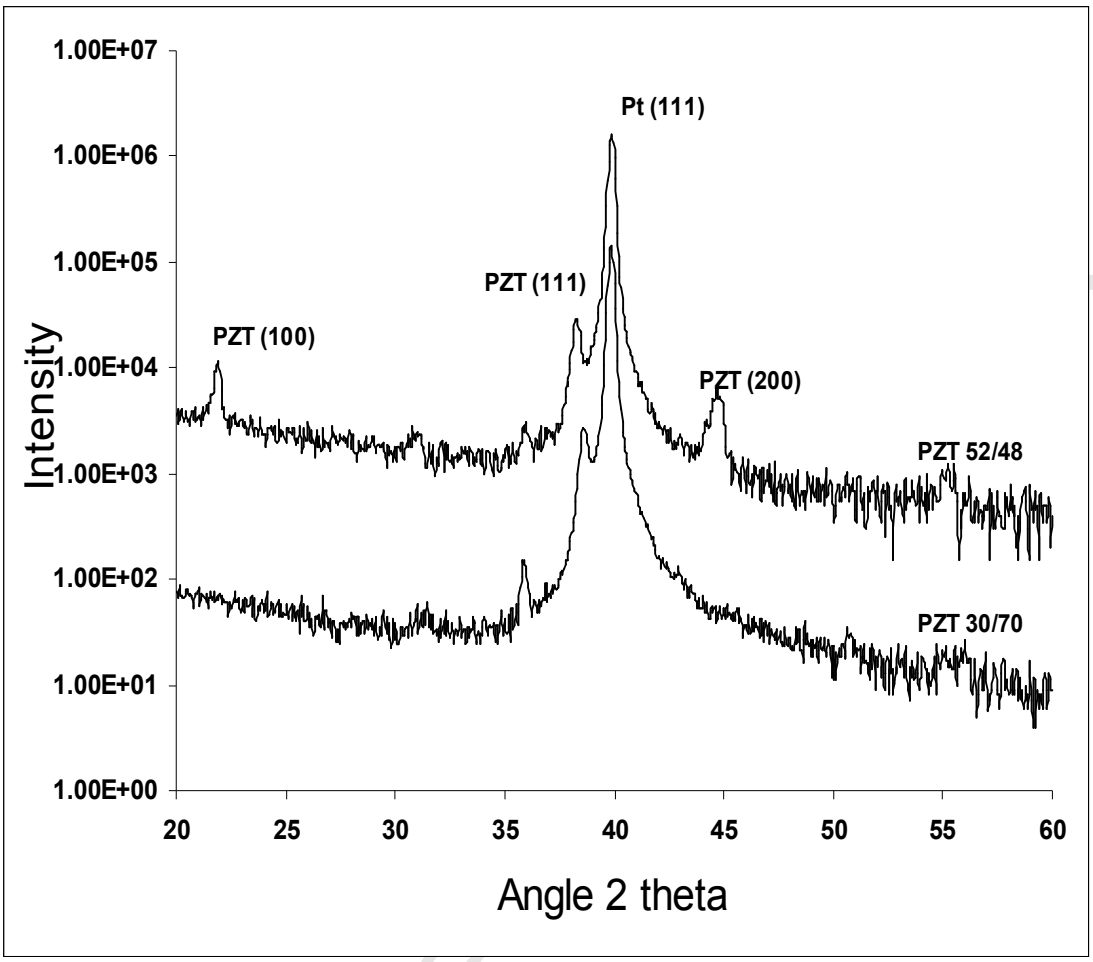

Figure 3

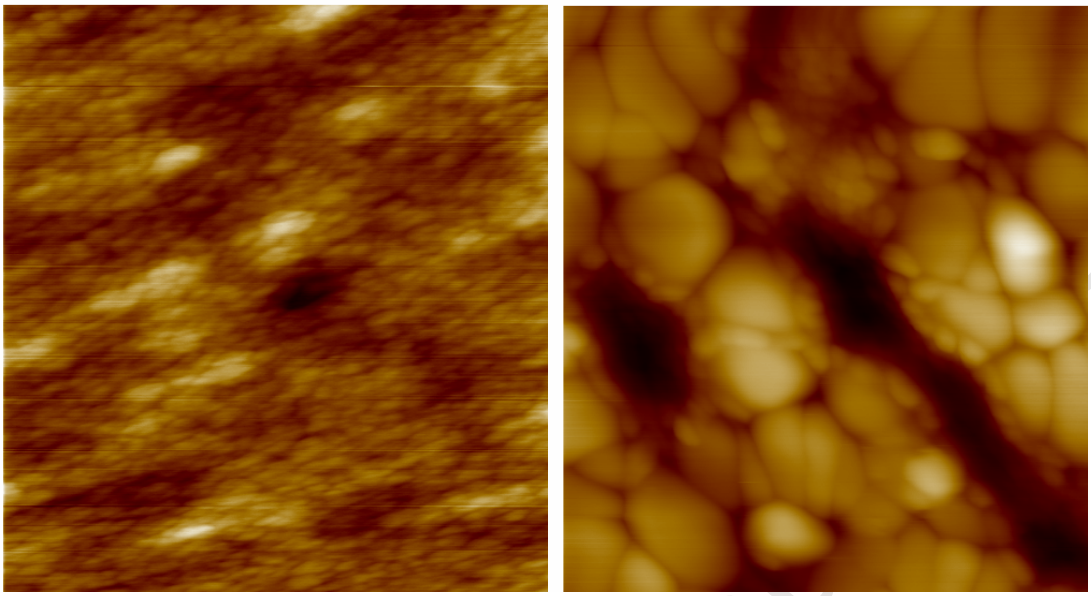

Figure 4

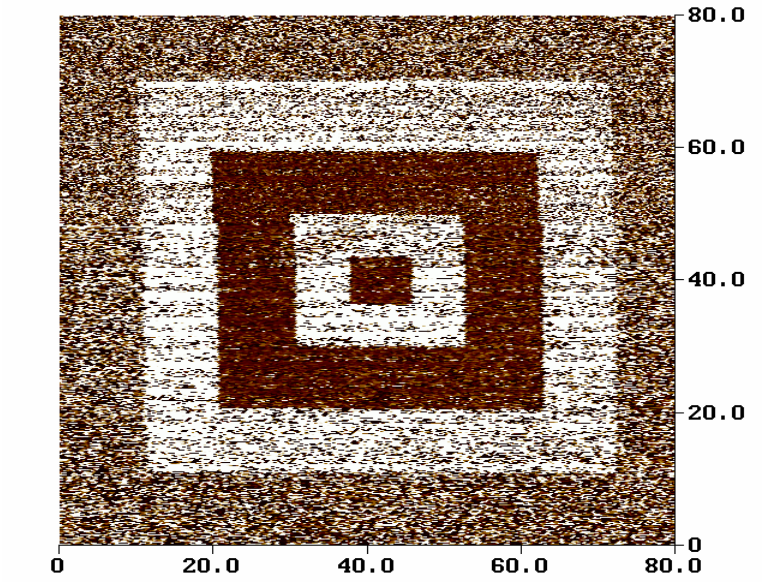

Figure 5

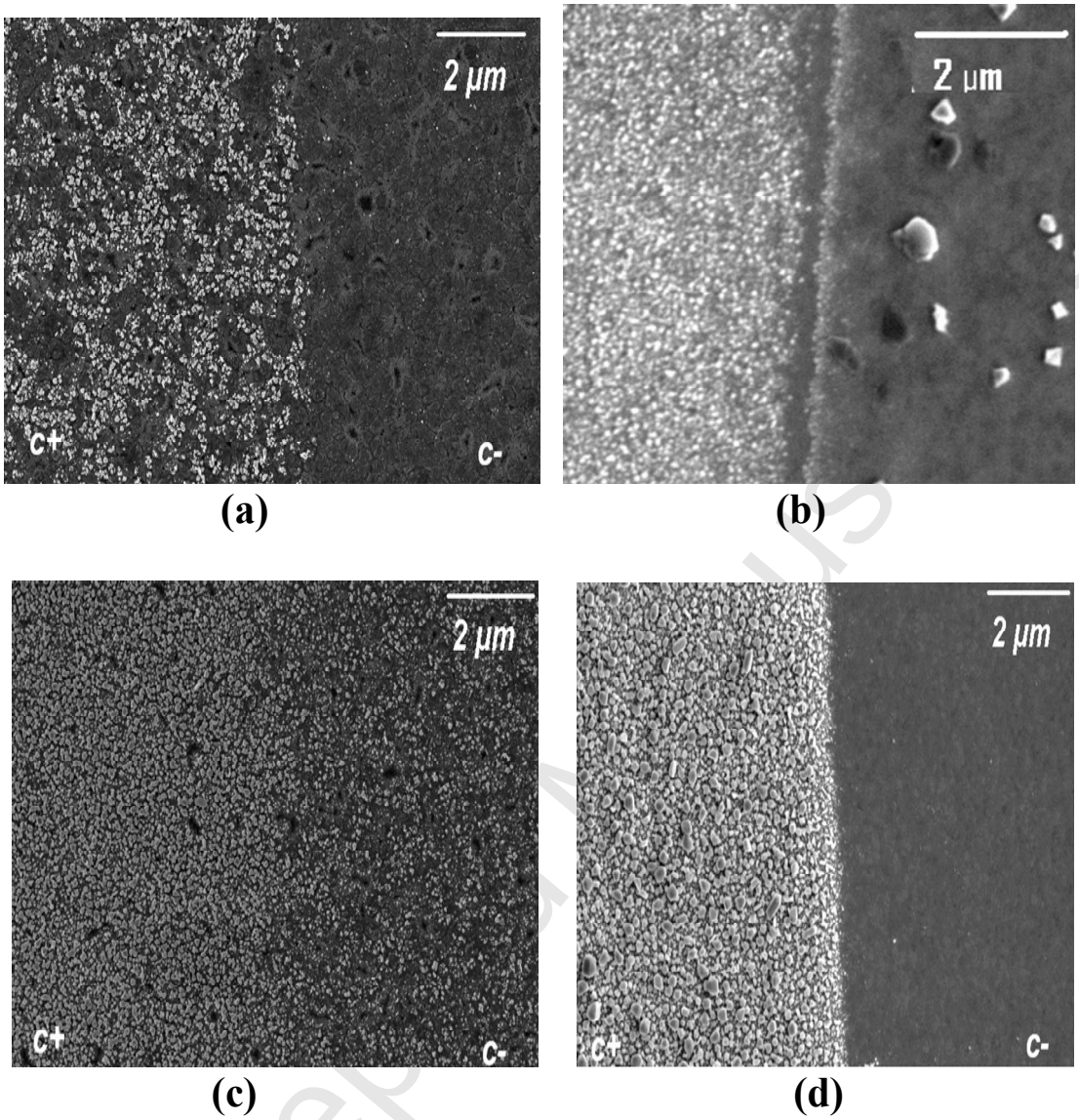

Figure 6

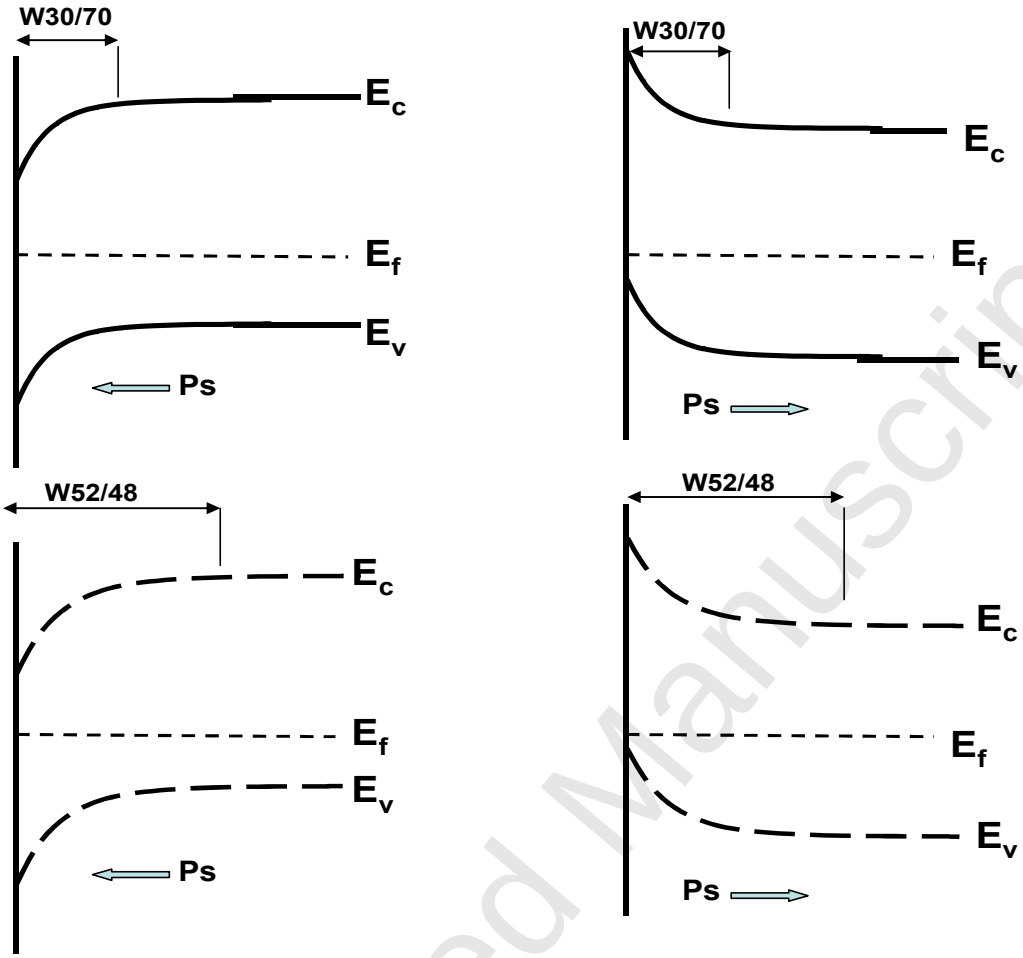

Figure 7